A comparative high-resolution study of predissociation linewidths in the Schumann-Runge bands of O_2

P. M. Dooley, B. R. Lewis, S. T. Gibson, K. G. H. Baldwin, P. C. Cosby, J. L. Price, R. A. Copeland, T. G. Slanger, A. P. Thorne, J. E. Murray, and K. Yoshino

A comparative high-resolution study of predissociation linewidths in the Schumann-Runge bands of O_2

P. M. Dooley, B. R. Lewis, S. T. Gibson, and K. G. H. Baldwin
Research School of Physical Sciences and Engineering, The Australian National University, Canberra ACT 0200, Australia

P. C. Cosby, J. L. Price,[a] R. A. Copeland, and T. G. Slanger
Molecular Physics Laboratory, SRI International, Menlo Park, California 94025

A. P. Thorne and J. E. Murray
Blackett Laboratory, Imperial College of Science, Technology, and Medicine, London SW7 2BZ, United Kingdom

K. Yoshino
Harvard-Smithsonian Center for Astrophysics, Cambridge, Massachusetts 02138

Results are presented of a comparative study in which three distinct high-resolution experimental techniques (vacuum-ultraviolet laser spectroscopy, laser-induced fluorescence spectroscopy and vacuum-ultraviolet Fourier-transform spectroscopy) were used to study predissociation in the Schumann-Runge bands of O_2 $B\,^3\Sigma_u^-(v')\leftarrow X\,^3\Sigma_g^-(v'')$ with $v'=13$ and 14. Our measurements are the first to be performed at high resolution for these levels and represent a significant advance on previous knowledge, characterizing completely the fine-structure and rotation dependencies of the $B\,^3\Sigma_u^-(v=13$ and 14)-state predissociation for the first time. The measured fine-structure-specific linewidths will result in significant improvements in the parameterization of models describing predissociation of the B-state and will have an impact on the development of realistic photochemical models of the terrestrial atmosphere. Good agreement was found between linewidths measured using vacuum-ultraviolet laser spectroscopy and laser-induced fluorescence spectroscopy, but unexpected difficulties arose in determining quantitative linewidths using vacuum-ultraviolet Fourier-transform spectroscopy. For each experimental technique, the instrumental resolution had to be carefully controlled and monitored in order to ensure reliable interpretation of the measured spectra. © *1998 American Institute of Physics.* [S0021-9606(98)00734-X]

I. INTRODUCTION

Photodissociation in the Schumann-Runge (SR) band system of molecular oxygen, $B\,^3\Sigma_u^-\leftarrow X\,^3\Sigma_g^-$ (175–205 nm), is a major source of odd oxygen in the stratosphere and the dominant one in the mesosphere. In addition, photoabsorption in the SR bands controls the depth of penetration of solar vacuum-ultraviolet (VUV) radiation into the atmosphere. Thus, due to their important role in terrestrial atmospheric photochemistry, the SR bands have been the subject of considerable study. The B state is predissociated by a number of repulsive states correlating with two ground-state oxygen atoms[1,2] and an accurate knowledge of the vibration, rotation and fine-structure dependence of the corresponding predissociation linewidths is essential,[3] both for the construction of realistic photochemical models,[4] and for the accurate parameterization of the predissociation mechanisms.[1,2]

Although there have been many attempts to measure predissociation linewidths in the $(v',0)$ SR bands, there remain significant disagreements between linewidths obtained in different laboratories.[5] This contrasts with the situation for the

measured SR-band oscillator strengths[6,7] for which good agreement has been found. The most extensive measurements on the vibration and rotation dependence of the predissociation linewidths are those of Lewis *et al.*[8] and Cheung *et al.*[9] The results of Lewis *et al.*[8] ($v'=1-19$) were obtained from equivalent-width measurements taken using a 2.2 m VUV monochromator with an instrumental resolution of 4.5 pm (~1.4 cm^{-1}) full-width at half-maximum (FWHM), while those of Cheung *et al.*[9] ($v'=1-12$) were obtained from the near-absolute photoabsorption cross-section measurements of Yoshino *et al.*,[7,10,11] taken using a 6.65 m scanning spectrometer with an instrumental resolution of 1.3 pm (~0.4 cm^{-1}) FWHM. The $\sim20\%$ discrepancy between these two sets of fine-structure-averaged linewidths for $v'=1-12$ has been reduced recently to $\sim8\%$ by a reanalysis[5] of the measurements of Yoshino *et al.*, using cross sections of improved accuracy[12] and a less constrained method of data analysis.

In order to characterize accurately the B-state predissociation, it is preferable to measure fine-structure-specific linewidths. However, for many bands in the SR system, principally the broader bands with $v'=1-12$, the P- and R-branch triplets are incompletely resolved because the splittings of the ground- and upper-state triplet components F_1,

J. Chem. Phys., Vol. 109, No. 10, 8 September 1998

Dooley *et al.* 3857

F_2, F_3 are similar and the linewidths are comparable with the fine-structure splittings. In addition, near $v'=6$ the P and R branches in the $(v',0)$ spectra overlap, further inhibiting the confident determination of fine-structure-specific linewidths. A substantial improvement in the separation of fine-structure components was achieved by Cosby *et al.*,[13] using absorption from higher vibrational levels of the ground state $X\,^3\Sigma_g^-$ to access the B-state. In addition, their use of laser-induced fluorescence (LIF) to detect the absorptions served to amplify[14–16] even small differences among the predissociation rates of the B-state fine-structure levels, allowing the measurement of fine-structure-specific predissociation rates for an extended range of rotational levels with $v'=0,2$ at high resolution (~ 0.06 cm$^{-1} \approx 0.4-0.8$ pm FWHM).

For $(v',0)$ transitions, the fine-structure separation is sufficient for the narrower $v' \geq 13$ levels to allow the resolution of individual components with an instrument of sufficient resolving power, but such measurements are rare. Lewis *et al.*[17] have deduced predissociation linewidths for resolved F_1 levels with $v'=17$, $N'=2-26$ from high-resolution (~ 0.15 cm$^{-1} \approx 0.5$ pm FWHM) photoabsorption spectra obtained using a coherent VUV source based on high-order anti-Stokes stimulated Raman scattering in H_2 of pulsed dye-laser radiation. In the absence of explicit spectral resolution, a determination of fine-structure-specific linewidths requires some form of synthetic spectral modeling. Indeed, the analysis by Lewis *et al.*[5] of the cross sections measured by Yoshino *et al.*[12] have enabled the determination of some fine-structure-specific widths for $v'=1$, 2, 5, 7–13, through such deconvolution procedures.

We have undertaken a collaborative study to address the lack of high-resolution measurements of fine-structure-specific predissociation linewidths in the SR bands, in order to characterize precisely the mechanisms for predissociation of the B state, and to provide accurate data for use in photochemical models of the terrestrial atmosphere. Three entirely different state-of-the-art high-resolution experimental techniques are used in different laboratories: vacuum-ultraviolet laser spectroscopy (VUVLS) at the Australian National University (ANU); laser-induced fluorescence spectroscopy (LIFS) at SRI International; and synchrotron-based vacuum-ultraviolet Fourier-transform spectroscopy (VU-VFTS) at the Photon Factory. In this work, we compare critically these three experimental techniques and illustrate the comparison with rotation- and fine-structure-specific studies of the $B\,^3\Sigma_u^-(v=13$ and 14) levels using each technique. These levels are among the narrowest in the SR system, providing an ideal testing ground for the high-resolution spectroscopies employed.

A preliminary report on the VUVLS measurements[18] and the results of a VUVLS study of perturbations in the high-v' SR bands[19] have appeared elsewhere. Details of an improved predissociation model for the B state, resulting from a combination of all of the new fine-structure-specific data, will appear in a further paper.

II. EXPERIMENTAL METHODS

A. Vacuum-ultraviolet laser spectroscopy

The experimental apparatus for VUVLS has been described in detail elsewhere.[19] Briefly, two-photon-resonant difference-frequency four-wave mixing[20,21] (2PR-DF4WM) of excimer-pumped dye-laser radiation in Xe was used to generate tunable narrow-bandwidth VUV radiation from 177.5 nm to 180.6 nm, in order to measure high-resolution photoabsorption cross sections for all accessible rotational lines from the (13,0) and (14,0) SR bands.

Two dye lasers (Lambda Physik FL3002E) were pumped by a common XeCl excimer laser (Lambda Physik EMG201). The output of the first dye laser, operated with the dye Coumarin 307, was frequency doubled in a BBO I crystal and the doubled output was tuned to be two-photon-resonant with the $6p[\frac{5}{2}]_2$ level of Xe at 78 120 cm^{-1}. This beam was combined with the tunable output of the second dye laser and both beams were focused into a cell containing Xe by an off-axis lens. Tunable VUV radiation generated by the 2PR-DF4WM process was passed through a low-resolution monochromator which discriminated against unwanted wavelengths. The dyes Coumarin 47 and 120 were used in the second dye laser, allowing tunability in the range 440–459 nm, and resulting in the production of VUV radiation in the range 177.5–180.6 nm. The VUV radiation leaving the monochromator was divided into two beams by a beam splitter. The reflected beam was monitored directly, while the transmitted beam passed through an absorption cell of length 33 cm, equipped with MgF$_2$ windows, before being detected. Output pulses from solar-blind monitor and detector photomultipliers were processed by a boxcar averaging system. The dynode-chain voltage of each photomultiplier was reduced, in order to limit the peak signal current to a value such that detector nonlinearity due to space-charge effects was $<1\%$. Most aspects of the experimental procedure were computer controlled, including triggering of the excimer laser, synchronous scanning of the dye laser and VUV monochromator, gas handling, pressure measurement and data acquisition.

All measurements were performed at room temperature (293 K). The phase matching for the 2PR-DF4WM process was optimized by careful beam alignment and by adjusting the pressure of Xe, normally in the range 70–90 Torr, to maximize the VUV signal for the particular scan range. The lasers were operated at a 10 Hz repetition rate and the monitor and detector signals were averaged over 50 laser shots for each datum point. The experimental scans varied from 1 cm^{-1} to 10 cm^{-1} in extent, with wave-number increments in the range 0.015–0.03 cm^{-1}. Scans were performed in groups of three, with the absorption cell alternately filled with a pressure of O_2 (99.9% purity) in the range 0.5–100 Torr, then evacuated, then refilled. This scheme compensated for drifts in photomultiplier sensitivity and the effects of wavelength structure in the photomultiplier signals which was not related to O_2 absorption.[22] Division of the detector signal by the monitor signal, after correction for scattered radiation, compensated for the shot-to-shot fluctuations inherent in the generated VUV signal. Absolute cell transmit-

tances were obtained by dividing the full-cell ratios (detector/monitor) by the empty-cell ratios at each wavelength. Photoabsorption cross sections were calculated from the absolute transmittances using the Beer–Lambert law.

Each dye laser was operated with an intracavity étalon to minimize the VUV bandwidth. The nominal VUV wave number was given by

$$\nu_{\text{vuv}} = \nu_{2p} - \nu_{\text{vis}}, \qquad (1)$$

where ν_{2p} was the wave number of the Xe two-photon resonance and ν_{vis} was the vacuum-corrected wave number of the tunable dye laser. The measured wave numbers of Yoshino *et al.*[23] for selected sharp, unblended lines of the SR system (accuracy ~ 0.1 cm^{-1}) were used for absolute wave-number calibration in the VUV. Linewidth uncertainties due to uncertainties in the relative wave-number calibration of an étalon scan are expected to be negligible.[19]

The spectral characteristics of the generated VUV radiation are of central importance in evaluating the reliability of linewidth measurements made with the VUVLS system, meriting discussion in some detail. The factors determining these spectral characteristics include: the bandwidth of the fundamental radiation produced by the two dye-laser oscillators; the modification to the oscillator spectral output by the two-stage pulse amplification and (in the case of the two-photon-resonant laser) by second-harmonic generation; the effect of the nonlinear four-wave mixing process; and, finally, modification of the nonlinear output due to the presence (under some circumstances) of intense laser fields.

The dye lasers used contain an oscillator and two amplifier stages. The oscillator cavity comprises a grating in Littrow configuration at one end and a dielectric mirror at the other. A series of prisms beam-expands the radiation from the pump region onto the grating to maximize the number of grating rulings illuminated. A specular reflection from one of the prisms forms the output-coupled beam, which is in turn reflected from a different portion of the grating to disperse any unwanted amplified spontaneous emission (ASE). The primary frequency-selective element is a Fabry–Perot étalon inserted into the cavity between the grating and the prisms. The étalon has a free spectral range of 1 cm^{-1} and modest finesse, yielding a bandwidth of <0.04 cm^{-1} FWHM. The cavity length is ~ 30 cm which gives a longitudinal cavity-mode spacing of 0.016 cm^{-1}, thereby enabling up to three cavity modes to be present within the étalon bandwidth. The oscillator is normally adjusted to favor a single cavity mode at the center of the étalon bandpass, with two much weaker longitudinal side modes being present. In practice, a combination of mode competition and thermal and mechanical instabilities results in shot-to-shot variations in the mode positions. Thus, the average spectral profile of the oscillator output resembles a series of mode peaks whose envelope is determined by the bandwidth of the étalon. Some gain narrowing may also occur, reducing the spectral intensity in the line wings. Such a narrow, multimode-envelope laser output has been observed in our laboratory using a pulsed spectrum analyzer (Burleigh PLSA3500).

The output from the oscillator is amplified twice in single-pass amplifiers, the latter of which is usually satu-

rated. For the measurement of photoabsorption cross sections, however, the amplifier pump beams are attenuated to reduce the effects of ac Stark broadening in the Xe nonlinear medium. Nevertheless, some gain narrowing and chirping of the laser pulse is to be expected which will further modify the laser spectral output, although the relative frequency shifts involved are only of the order of 10^{-7}.[24] Spectral chirping may also occur in the frequency-doubling process as a result of the fact that the fundamental laser pulse is itself temporally asymmetric and chirped. The distortion of the temporal pulse shape due to the nonlinear response (proportional to the square of the instantaneous spectral intensity) thereby modifies the frequency distribution of the second harmonic.[25]

A similar frequency modification can occur in the four-wave mixing process. In particular, the two-photon-resonant process will exhibit the same type of sensitivity to the instantaneous phase of the fundamental radiation as occurs in second-harmonic generation. In addition, further modification of the VUV bandwidth may arise from ac Stark effects on the Xe energy levels, including broadening, shifting and asymmetry.

Thus, due to the complications described above, the VUV bandwidth is unlikely to be related simply to the fundamental laser bandwidths. Hepburn[26] has reported a VUV bandwidth of three times that of the input lasers (0.16 cm^{-1} FWHM) for four-wave mixing in Hg and Mg vapor, once the tuning of the two-photon-resonant laser had been optimized. On the other hand, Yamanouchi and Tsuchiya[21] reported a VUV bandwidth of 0.06 cm^{-1} FWHM for 2PR-DF4WM in Sr vapor, not much greater than the input bandwidths. Our observed VUV bandwidths were intermediate between these values, varying significantly in the range 0.06–0.12 cm^{-1} FWHM according to the details of the particular experimental set-up adjustments.

In addition, it was found that ASE provided an unexpected means of instrumental distortion of the photoabsorption line shape. ASE from either dye laser, in combination with the other tuned beam, produced an untuned ASE pedestal in the generated VUV signal. Since the bandwidth of the VUV monochromator greatly exceeded that of the tuned component of the VUV signal, the broadband ASE VUV signal was favored disproportionately in the detection process, acting effectively as a scattered-light component. Thus, if the center of a narrow line were totally absorbed, the observed transmittance flattened off at a nonzero value, resulting in an underestimate of the peak photoabsorption cross section and a corresponding modification of the line shape.

In order to monitor the unpredictable instrumental bandwidth and eliminate the ASE problem, the following procedure was adopted. A narrow SR line, the $R_1(21)$ line from the (14,0) band, was chosen as a reference line. The oscillator strength for this line is well known from conventional spectroscopic measurements,[6] but independent knowledge of its predissociation linewidth was required for its full characterization. This was obtained by measuring the integrated absorptivity of the reference line for a range of O_2 pressures, yielding an experimental curve of growth.[27] A Voigt curve-of-growth analysis, using the known oscillator strength and a

Gaussian width Γ_G defined by the Doppler component, after correction for the effects of collision-induced broadening,[28,29] yielded a Voigt mixing parameter $a = \sqrt{\ln 2}\,\Gamma_L/\Gamma_G = 0.35$, implying a Lorentzian width Γ_L, due to predissociation, of 0.051 ± 0.007 cm^{-1} FWHM. Since equivalent width is independent of instrumental resolution,[27] this determination of the reference predissociation linewidth required no assumptions regarding the instrumental VUV bandwidth.

Once the reference line was characterized fully, it was scanned daily in order to optimize the experimental adjustments and determine the instrumental bandwidth. This was a difficult procedure. First, it was necessary to minimize the effects of ac Stark broadening by progressively reducing the dye-laser intensities until the apparent width of the reference line showed no intensity dependence. Second, it was essential to minimize ASE in the VUV signal. This was achieved by maximizing the apparent peak absorption of the reference line while iteratively adjusting the experimental system. These adjustments included: rotating the pump-beam line foci so as to be noncollinear with the laser beam; aligning the two laser beams into the Xe cell to maximize the efficiency of the 2PR-DF4WM process, thereby enabling operation at reduced laser intensities; and further attenuation of the pumping of the three dye-laser stages, as necessary. Following this system optimization, line-shape distortions due to ASE had been eliminated and it was possible to deduce a daily value for the VUV bandwidth using the least-squares fitting procedure described in Sec. III, together with the known strength and width parameters for the reference line. It was established that this bandwidth remained unaltered during the subsequent period of data taking. However, it was necessary to reoptimize the system daily, with a consequential change in bandwidth, unpredictable within the $0.06–0.12$ cm^{-1} FWHM range.

As is apparent from the discussion above, it is difficult to define accurately the instrumental line shape *a priori*. Analyses of the reference line using a Gaussian profile to describe the shot-averaged instrumental line shape provided good fits to the experimental cross sections. Therefore, a Gaussian profile was assumed for the analysis of all measured cross sections.

B. Laser-induced fluorescence spectroscopy

The experimental protocol for LIFS has recently been described in detail,[13] so only the salient features and some important modifications will be discussed here. The O_2 B-state level is excited by single-photon absorption from an excited vibrational level of the O_2 X $^3\Sigma_g^-$ ground state and is monitored by detecting the weak $B \rightarrow X$ fluorescence that competes with predissociation. Two laser beams, pump and probe, are required for the experiment. The pump-laser beam creates vibrationally excited O_2 by photolysis of O_3,[30] while the narrow-band probe-laser beam, temporally delayed with respect to the pump beam, is tuned in wavelength to excite the $B \leftarrow X$ absorption. All measurements were made at room temperature in a dilute mixture of O_3 in He at a total pressure in the range 20–30 Torr.

The probe-laser beam was generated by a dye laser (Lambda Physik LPD3000E) pumped by a XeCl excimer laser (Lambda Physik EMG102). When low powers were required, this dye laser was generally operated using only its oscillator and (attenuated) amplifier stages. A $3\times$ beam-expanding telescope served to produce a collimated output beam which was further restricted by a 3 mm diameter aperture before entering the experimental cell. Two beam splitters between the laser and the cell directed portions of the excitation-laser beam to a monitor étalon, for verification of the laser-mode purity, and to an I_2 (LIF, $\lambda > 500$ nm) or Te_2 (absorption, $\lambda < 500$ nm) cell for wavelength calibration. For measurements of the SR (13,15), (13,16), and (14,16) bands, the frequency of the laser was doubled in a KDP crystal positioned between the beam splitters and the cell. Exalite 428 or Coumarin 120 dye solutions were used to generate the blue wavelengths for direct pumping of the SR (13,26), (13,27), and (14,26) bands, while Rhodamine 590 dye solution was used to generate the fundamental wavelengths for those bands requiring use of the doubling crystal. An intracavity étalon was used in the oscillator of the probe dye laser, which produced an (approximately Gaussian) instrumental bandwidth at the blue wavelengths in the range $0.04–0.05$ cm^{-1} FWHM, as indicated both by the observed widths of the unblended peaks in the Te_2 absorption spectrum and by analysis of the SR absorption line shapes. The linewidth of the doubled laser was typically a factor of $\sqrt{2}$ larger than this, as verified by the observed (Doppler-corrected) widths of LIF peaks due to impurity OH absorptions in the O_3/He sample and by analysis of the SR absorption line shapes. Laser powers entering the cell were typically in the range 1–10 μJ, as required to minimize saturation broadening of the absorption lines. For the work reported here, the delay in the probe-laser pulse relative to the pump-laser pulse was in the range 1–10 μs, with the shortest delays favoring excitation from the higher ($v'' = 26$ and 27) vibrational levels of the O_2 X state.

The pump laser was the KDP-doubled output of a YAG-pumped dye laser (Quantel TDL-50), which provided a photolysis wavelength of 281 nm with pulse energies in the range 2–5 mJ. Although photolysis of O_3 is less efficient at this wavelength than at the excimer-laser-produced 248 nm used in previous work,[13] the pulse energy stability of the YAG-pumped system was found to be far superior in maintaining a uniform population of vibrationally excited O_2. The photolysis beam was apertured to 3 mm diameter, weakly focused through the cell, and precisely adjusted to counter-propagate collinearly with the probe beam, so as to maximize the LIF signal.

Fluorescence from the $B(v' = 13$ and 14) levels in the (13,3–6) and (14,3–6) emission bands was detected by a solar-blind photomultiplier through a MgF_2 window and an interference filter centered at 206 nm with a bandpass of 26 nm FWHM. A second photomultiplier with a blue-sensitive photocathode (R212), positioned at right angles to the first, simultaneously viewed the interaction region through a Suprasil window and a Wratten 18A filter (centered at 350 nm) with a bandpass of approximately 50 nm FWHM. Both the doubled pump beam and the probe beam were linearly polarized with the direction of polarization of the doubled ex-

citation beam and the photolysis beam orthogonal to the direction viewed by the solar-blind photomultiplier. In contrast, the polarization of the undoubled probe beam was in the direction viewed by this photomultiplier. However, no spatial inhomogeneity was observed in the detected fluorescence, such as might have been produced by alignment of the emitting O_2 with respect to the probe-laser polarization direction.

The amplified outputs of the photomultipliers were detected by boxcar integrators, whose digitized outputs were transferred to a laboratory computer after each laser shot, together with the signals from the monitor étalon, the wavelength calibration cell, and the probe-laser power meter. The computer also controlled the wavelength of the probe laser. Both lasers were operated at a repetition rate of 10 Hz and the probe laser was stepped in wavelength by $0.005-0.010$ cm^{-1} after the accumulation of 10, 20, or 30 laser shots. Scans typically ranged from 6 cm^{-1} to 30 cm^{-1} in extent. All scans were wave-number calibrated using the I_2 (Ref. 31) or Te_2 (Ref. 32) reference lines, yielding accuracies of 0.013 cm^{-1} and 0.008 cm^{-1} for the doubled and undoubled probe beams, respectively.

The variation in 206 nm fluorescence intensity as a function of probe-laser wavelength constitutes the $B \leftarrow X$ absorption spectrum observed by LIFS. Prior to analysis, the raw fluorescence intensity at each wavelength was linearly corrected for small ($<10\%$) relative changes in the probe-laser power that may have occurred during the course of a scan and any wavelength-independent intensity contribution was subtracted. As discussed previously,[13] the absorption line shapes are subject to saturation broadening and (at much higher probe powers than used here) to a depletion in the population of the absorbing level of the X state of O_2. Therefore, the line shapes of selected rotational features in each of the SR bands were monitored as a function of probe-laser energy. These empirical changes in line shape were fully consistent with those expected from the measured (spatially averaged) laser energy densities and the stimulated emission coefficients of the various bands.[13] All measurements reported here were obtained with probe-laser energies that were sufficiently low that the required corrections for residual saturation broadening were $<10\%$ of the Lorentzian component in the Voigt line shape.

C. Vacuum-ultraviolet Fourier-transform spectroscopy

The spectral region of application of Fourier transform spectroscopy (FTS) has been extended into the VUV at Imperial College by means of an interferometer designed specifically to work at these shorter wavelengths.[33] The cut-off of the prototype interferometer was set at about 180 nm by the fused-silica beam splitter employed, but the substitution of a MgF_2 beam splitter has increased the range to about 140 nm.[34] The limiting resolution of this instrument is 0.025 cm^{-1} FWHM, more than sufficient to resolve the Doppler widths of the lines of the SR bands.

The attainment of a good signal-to-noise ratio (S/N) in high-resolution absorption spectroscopy is much more demanding than in emission spectroscopy because of the noise characteristics of the technique. Every spectral element seen by the detector contributes to the noise in the interferogram, and if the noise is ''white'' (independent of frequency) it is distributed evenly through the spectrum by the Fourier transform. In the UV, the dominant noise is photon noise, proportional to the square root of the signal. The S/N in the spectrum for a quasi-continuum is proportional to $(\phi t/W)^{1/2}$, where ϕ is the detected photon flux in photons s^{-1} nm^{-1}, t (s) is the total integration time and W (nm) is the bandwidth. There are, therefore, two requirements for high S/N: a background continuum source of high photon flux, and some means of limiting the spectral bandwidth to the region of interest to avoid all unnecessary contributions to the photon noise. Ordinary laboratory continuum sources (the high pressure Xe arc, the deuterium lamp and the argon mini-arc) fall off rapidly in radiance below 200 nm. The only alternative is synchrotron radiation. As this is intrinsically very broadband, the bandwidth must be limited either by optical filters or by a monochromator. Interference filters are inflexible and inefficient in the VUV, so the preferred option is a monochromator. Ideally, this should be a double monochromator with zero net dispersion, because the spread of angles passing through the interferometer from a single monochromator leads to small wavelength shifts and phase problems across the pass band.

Recent measurements of absorption cross sections of the $\delta(0,0)$ and $\beta(7,0)$ bands of NO by FTS at IC (Ref. 35) demonstrated these problems. With the continuum source used (a 500 mA positive-column discharge in hydrogen, similar to, but brighter than, a commercial deuterium lamp) the S/N obtainable for the $\delta(1,0)$ band at 183 nm was inadequate. The 0.3 m Czerny-Turner monochromator used as predisperser generated, as anticipated, uncomfortably large phase variations across the pass band. It was therefore decided to attempt to use synchrotron radiation as the background continuum for the absorption measurements on the SR bands. The particular choice of the Photon Factory was dictated by the availability on one of the beam lines of a zero-dispersion monochromator, normally used as the predisperser for the 6.65 m off-plane Eagle spectrograph of Dr. K. Ito,[36] who collaborated with us on the project.

Following shipment of the IC VUV FT spectrometer to Japan, the instrument was set up downstream of the monochromator. The rectangular beam normally falling on the entrance slit of the 6.65 m spectrograph was intercepted by a cylindrical mirror that focused it as an approximately circular patch of diameter 2 mm on the circular entrance aperture of the interferometer, after passing through an absorption cell 78 mm long. The pressure of O_2 was set at a value between 0.6 Torr and 10 Torr, depending on the spectral region observed. The bandwidth of the predisperser was normally set at 2.5 nm. Alignment of the interferometer axis with the synchrotron beam reflected by the cylindrical mirror proved to be a difficult task; good fine adjustments to position and rotation were not available during the limited period at Photon Factory, and the problems were accentuated by the fact that the VUV beam emerging from the double-grating monochromator was not coincident with the visible light beam when the gratings were turned to zero order. The possibility of small misalignments, or drifts in alignment, was a source

of some anxiety and is discussed further in Sec. III C. Most spectra were taken at a resolution of 0.06 cm^{-1} FWHM, but for some spectra the resolution was set at 0.12 cm^{-1} FWHM in order to maximize the S/N. This latter value matches the Doppler width for O_2 at room temperature. It should be noted that the S/N is proportional to the resolution if all other factors are held constant; if the maximum allowable entrance aperture is used and filled, the S/N in the photon-noise limit actually scales with the 3/2 power of the resolution. Thus, a factor of 2 in resolution requires a factor of 8 in integration time to recover the same S/N.

The synchrotron flux was attenuated by two mirror and two grating reflections plus transmission through four uncoated MgF_2 windows before entering the interferometer, where it underwent six further mirror reflections, one further window transmission, and a reflection/transmission at the beam splitter. The photon flux was estimated to be about 10^{10} photons nm^{-1} s^{-1} at the entrance to the interferometer, and about 10% of this on the detector (an R1220 photomultiplier with a solar-blind photocathode and a MgF_2 window). The S/N is proportional to the modulation efficiency of the interferogram as well as to the square root of the photon flux, and both modulation and mirror reflectivities fall off rather steeply with decreasing wavelength in the VUV. It was necessary to integrate for many hours to obtain a good S/N. The integration was performed by coadding interferograms (each of which involved a scan time of 6–8 min) in piles of 30 or so. The individual piles were coadded into larger piles whenever inspection showed no sign of a drift in phase between piles; otherwise each pile was transformed and phase-corrected separately, and the spectra were subsequently coadded. Typically, two or three spectra taken over two 12 h days went into producing a spectrum 2.5 nm wide at a resolution of 0.06 cm^{-1} with a S/N in the continuum of around 40.

In addition to the SR bands, we also measured absorption in NO from 190 nm down to 160 nm with a resolution of 0.06 cm^{-1}, except for the bands of shortest wavelength for which the resolution was 0.12 cm^{-1}.

III. ANALYSIS

In the general case, spanning the range of experimental conditions represented by the three experiments described in Sec. II, three broadening processes may make significant contributions to the instrument-free SR photoabsorption line shape.[37] First, for distances not too far from the line centers, the predissociation line shape for unperturbed lines may be taken as Lorentzian.[1,2,19] Second, for O_2 pressures that are not too high, the collisional line shape may also be described with sufficient accuracy by a Lorentzian.[28,29] Thus, the total Lorentzian linewidth is $\Gamma_L = \Gamma_p + \Gamma_c$, where Γ_p and Γ_c are the predissociation and collisional linewidths, respectively. For the most part, the O_2 pressures are low enough for collisional broadening to be neglected, but the VUVLS measurements for the weaker lines of higher rotational quantum number were taken at pressures up to 100 Torr, resulting in collisional linewidths up to 0.03 cm^{-1} FWHM.[28,29] Third, it is necessary to consider the Doppler component of the line shape which has a Gaussian profile (Doppler width Γ_D

$\approx$0.12 cm^{-1} FWHM at room temperature). Thus, the Voigt profile, a convolution of Lorentzian and Gaussian line shapes, may be used to describe each rotational line in the analysis procedure:[38] the Gaussian linewidth component Γ_G is given by the well defined Doppler width, while the Lorentzian linewidth component Γ_L is the sum of predissociation and collisional components. For most of the results presented here, the very high experimental resolution, together with the relatively low predissociation linewidths, enabled full resolution of individual rotational and fine-structure lines, allowing a simple Voigt line shape fitting procedure to be employed, independent of any band-model assumptions.

A. VUVLS analysis

In the analysis of the VUVLS results, a nonlinear least-squares procedure, in which a synthetic cross section based on the Voigt line shape was fitted to the measured photoabsorption cross section, was used to determine independently the position, oscillator strength, and Lorentzian linewidth component for each rotational line in a particular scan. In a few cases, when the resolution of low-rotation F_2 and F_3 components was insufficient to enable independent fitting, the ratio of the strengths of these two fine-structure lines was held fixed at a readily calculable value[39] in the fitting procedure. In a few other cases, it was necessary to correct for the contributions of weak lines from other SR bands which were obscured completely by the lines of interest. The pseudo-continuum underlying the SR bands, comprising the wings of more distant lines, was represented by a quadratic polynomial in wave number, the coefficients of which were also determined in the fitting procedure. Normally, a constant or linear background was sufficient to obtain a good fit to the measured cross section. The Gaussian instrumental bandpass function was included explicitly in the synthetic cross section, through a convolution with the calculated transmittance spectrum, reproducing the small degradation in cross section due to the finite instrumental resolution.

B. LIFS analysis

A somewhat similar procedure was also followed in the analysis of the LIFS line shapes. However, a significant difference arises in that the relative fluorescence intensities are not only directly proportional to the photoabsorption cross sections, but are also inversely proportional to the lifetimes of the emitting levels. Thus, there is a correlation between the fluorescence intensity and the linewidth of the Lorentzian component of the Voigt line shape that describes each feature in the LIF excitation spectrum.[13] The linewidth Γ_G of the Gaussian component of the Voigt line shape was taken as a combination, in quadrature, of the instrumental width (Sec. II B) and the 300 K Doppler width of the absorption at the probe-laser wavelength.[40] Since much longer absorption wavelengths were used to produce the B-state levels in the LIFS studies, this Doppler contribution was relatively small in comparison with that applying to the two other experimental techniques, amounting to only 0.05 cm^{-1} FWHM and 0.09 cm^{-1} FWHM at the blue and frequency-doubled probe-laser wavelengths, respectively. The value of Γ_G was taken to be constant for all features within a given scan.

The line shapes for each of the three fine-structure components of a given LIFS rotational line multiplet were analyzed simultaneously, with the ratios of their individual photoabsorption line strengths held constant at the calculated values.[41] A nonlinear least-squares fit of the three coupled Voigt line shapes to the observed LIF spectrum yielded values for the line center and Lorentzian linewidth Γ_L of each of the three fine-structure components. In addition, values for the common background intensity of the LIF spectrum in the region of the multiplet and for the average relative absorption cross section of the multiplet were also determined in the fit. The relative magnitudes obtained for this latter parameter among the rotational lines in a given absorption band were found to be consistent with those calculated for a 300 K rotational temperature. The values of Γ_L obtained from these fits, following a small correction for saturation broadening (Sec. II B), are reported here as the predissociation level widths.

C. VUVFTS analysis

The peak absorption for the strong lines in the VUV FT spectra was well over the linear limit. The transmittance spectra were converted to absorbance spectra by taking the logarithm and manually fitting a smooth curve to the continuum between regions of strong absorption. It should then have been possible to fit a Voigt profile to each line in the manner described in Sec. III A for the VUVLS results. The fitting procedure used was part of the GREMLIN suite of programs written by J. W. Brault specifically for the analysis of FT spectra.[42] Compared with the calculated Doppler width of 0.12 cm^{-1} FWHM, the instrumental width should be negligible for the spectra taken with 0.06 cm^{-1} resolution, and for those taken at 0.12 cm^{-1} the instrumental contribution can be allowed for by convolving an appropriate sinc function with the Voigt. Although the instrumental function should properly be applied to the transmittance spectrum rather than the absorbance, checks showed that there was a negligible difference to the final fit over the range of absorbance recorded here.

The fitting of the lines showed two anomalies. First, the Doppler component of the best-fit Voigt function had a FWHM in the range 0.15–0.17 cm^{-1}, significantly greater than 0.12 cm^{-1}. Clamping the Doppler width at the expected value gave a worse fit to the line profiles. Second, since the narrowest lines in the high-resolution spectra had a measured FWHM of about 0.23 cm^{-1}, all the lines should have been fully resolved even in the lower-resolution (0.12 cm^{-1}) runs. The measured widths in both sets should therefore have been similar, whereas in fact they were on average greater by some 0.03 cm^{-1} in the lower-resolution spectra.

In an attempt to throw some light on these anomalies, we compared the NO absorption spectra taken at the Photon Factory with those taken previously at Imperial College with the FT spectrometer and a hydrogen discharge continuum background.[35] The intrinsic line shape of the the $\delta(0,0)$ and $\beta(7,0)$ bands of NO is almost pure Doppler. Whereas in the previous spectra, the Doppler widths were, as expected, about 0.12 cm^{-1} FWHM for the room-temperature measure-

ments, the Photon Factory NO spectra appeared to have anomalous Gaussian widths similar to those in the O$_2$ spectra.

Comparison of the VUVFTS and VUVLS linewidths for a dozen well isolated O$_2$ lines showed that the FTS lines were consistently broader, on average by 0.06 cm^{-1} for the higher-resolution spectra and 0.09 cm^{-1} for the lower-resolution spectra. Taken together with the internal evidence, this suggests at first sight that the intrinsic resolution of the Photon Factory FT spectra was, for some reason, lower than the value determined by the length of the interferometer scan. We consider this explanation to be unlikely for two reasons. First, a broad instrumental function has less effect on a wide line than on a narrow one, whereas the VUVFTS-VUVLS differences for lines ranging in width from under 0.2 to 0.3 cm^{-1} FWHM (in the VUVLS spectra) show no dependence on linewidth. Second, to account for the observed broadening we have to postulate instrumental functions with widths of order 0.18 cm^{-1} and 0.21 cm^{-1} FWHM for the "high" and "low" resolution spectra, respectively. Convolution of the VUVLS spectra with sinc functions of these widths generates significant ringing, which is simply not observed in the VUVFTS spectra, so it is necessary to postulate further a smooth tapering off of the interferogram rather than a sharp termination. In that case the interferograms would be effectively truncated before the end of the shorter scans, and the additional scan length of the high-resolution interferograms would have no effect.

A possible explanation of the discrepancy is the "illumination shift" discussed by Learner and Thorne:[43] changes in the way in which the entrance aperture is illuminated affect the angular distribution of rays through the interferometer and result in small wave-number shifts. Given the inherent spatial instabilities of the synchrotron beam, the long optical path (two mirrors and two gratings) guiding it into the interferometer, the difficulties of aligning the latter and the many hours of coadding, it would indeed be surprising if there were not small illumination shifts. We have some evidence for them: if the separate piles of interferograms that make up one final spectrum are transformed separately, there are found to be small but significant wave-number shifts (0.01 to 0.03 cm^{-1}) between the piles in most cases. Unfortunately, the problem cannot be solved by simply correcting for these shifts because the lines within each pile are still anomalously wide, presumably due to shifts occurring during the accumulation of the pile. The maximum size of an illumination shift depends on the size of the entrance aperture and hence on the resolution. Illumination shifts of up to 0.03 cm^{-1} for the high-resolution, and somewhat more for the lower-resolution spectra would appear to be reasonable in the prevailing experimental conditions. However, the problem is that coadding a bunch of Voigt lines 0.2 cm^{-1} wide with displacements of up to 0.05 cm^{-1} or so does not broaden them enough to account for the observed widths.

We have to conclude that we do not have a satisfactory quantitative explanation for the anomalous widths of the VUVFTS lines. Since this problem has never before arisen over many years of use of the instrument on both emission and absorption spectra, it does appear to be related in some

way to the method of use at the Photon Factory. It has the unfortunate consequence that no reliable predissociation broadening parameters can be derived from the VUVFTS spectra without an independent measure of the effective instrumental resolution, although line strengths and relative wave numbers should not be affected.

IV. RESULTS AND DISCUSSION

Before proceeding further, it is pertinent to summarize some of the expected inherent advantages and disadvantages of each experimental technique. Both the VUVLS and VUVFTS techniques result in the measurement of photoabsorption cross sections, enabling absolute oscillator strengths, as well as predissociation linewidths, to be obtained from the measurements using the fitting technique described in Sec. III. VUVFTS has the advantage of simultaneous acquisition of the complete spectrum, but suffers from the need for a bright, controlled spectral-width continuum source in order to optimize the S/N. At present, this requires a synchrotron source. Both the VUVLS and LIFS methods require detailed, small step-size scans over the spectral features of interest and suffer from power-dependent bandwidths which must be controlled carefully. However, it is relatively easy to balance the conflicting requirements for a good S/N and a minimal power dependence of the bandwidth using the VUVLS method, since only moderate source intensity is required against which to measure the photoabsorption cross sections, whereas the LIF signal and S/N are directly related to the laser intensity. The LIFS technique has several unique advantages. First, as has been noted in Sec. III B, the photon energy is minimized by selecting a high vibrational level in the ground state as the origin of the absorbing transition. This, in turn, minimizes Doppler broadening of the transition, which scales directly with photon energy. Second, as mentioned in Sec. I, the ability to choose the lower-state level in the excitation allows a flexibility in controlling the separation of the fine-structure components in the absorption spectrum, which reflect the relative differences in the fine-structure levels of the B and X states. Third, the fluorescence intensity of the excited B-state level is inversely proportional to its lifetime. Thus, as we have noted in Sec. III B, the observed relative fluorescence intensities of the SR multiplets, in addition to their absorption line shapes, serve as another, more sensitive measure of their relative lifetimes. Finally, each B-state level can be accessed by absorption from two or more ground-state vibrational levels with different absorption cross sections, thus providing an important check on the influence of saturation broadening, or of unresolved line components, on the apparent line shape associated with the level. Overall, the high resolution provided by each experimental technique is expected to result in an important advance over all previous conventional measurements of SR linewidths.

We illustrate the observed characteristics of the different high-resolution experimental techniques in Fig. 1 which shows comparable measured and fitted spectra over the wave-number regions of the $B\ ^3\Sigma_u^-(v=14, N=12)$ fine-structure levels. Both the VUVLS and VUVFTS measure-
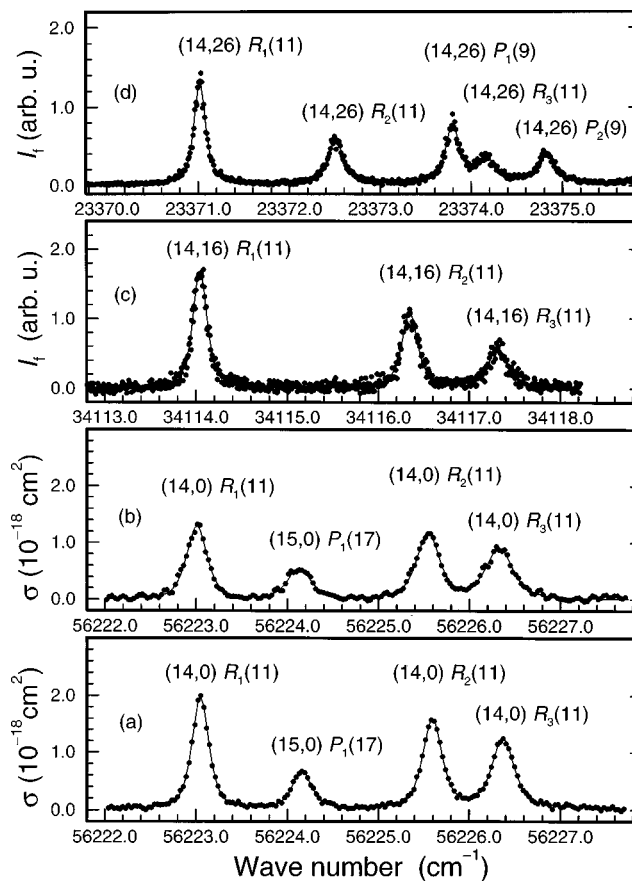

FIG. 1. Experimental scans (points) and fitted spectra (lines) over the region of the $B\ ^3\Sigma_u^-(v=14, N=12)$ fine-structure levels. (a) VUVLS cross section for $(14,0)\ R(11)$ triplet; Doppler width 0.12 cm^{-1}; instrumental resolution 0.10 cm^{-1}; apparent width for F_1 component 0.21 cm^{-1}; Lorentzian width 0.11 cm^{-1}. (b) VUVFTS cross section for $(14,0)\ R(11)$ triplet; Doppler width 0.12 cm^{-1}; instrumental resolution 0.19 cm^{-1}; apparent width for F_1 component 0.24 cm^{-1}; Lorentzian width 0.10 cm^{-1} (however, see the text). (c) LIFS scan for $(14,16)\ R(11)$ triplet; Doppler width 0.07 cm^{-1}; instrumental resolution 0.07 cm^{-1}; apparent width for F_1 component 0.18 cm^{-1}; Lorentzian width 0.12 cm^{-1}. (d) LIFS scan for $(14,26)\ R(11)$ triplet; Doppler width 0.05 cm^{-1}; instrumental resolution 0.05 cm^{-1}; apparent width for F_1 component 0.15 cm^{-1}; Lorentzian width 0.11 cm^{-1}. (All widths are FWHM values.) Each scan covers a similar range of wave numbers, but the lower transition energies for the LIFS scans result in smaller Doppler widths, and correspondingly smaller apparent linewidths.

ments are given in the form of effective photoabsorption cross sections σ for the $(14,0)\ R(11)$ fine-structure triplet, while the LIFS measurements are given in the form of relative fluorescence intensities I_f measured following excitation of the $(14,16)$ and $(14,26)\ R(11)$ fine-structure triplets. The differential wave-number scales of each spectrum are identical, allowing meaningful visual comparisons of apparent linewidths. A comparison of the two photoabsorption spectra indicates that the VUVLS cross section has a greater S/N and a higher resolution, as evidenced by greater peak cross sections and smaller apparent linewidths. This lower effective resolution for the VUVFTS cross section is unexpected, as has been discussed in Sec. III C. While the LIF spectra have a smaller S/N, the greater flexibility allowed by excitation of vibrationally excited ground-state levels is evident in the increased separation of the $R_2(11)$ and $R_3(11)$ components when compared with the photoabsorption spectra. In addi-

tion, it is clear from Fig. 1 that the relative intensities of the fine-structure components vary much more widely in the LIF spectra than in the photoabsorption spectra. As discussed above, this is a consequence of the dependence of the LIF signal on the predissociation lifetime and indicates, more directly than do the apparent (total) relative linewidths, that the predissociation linewidths vary significantly with the fine-structure component, in the order $\Gamma_p(F_1) < \Gamma_p(F_2) < \Gamma_p(F_3)$. Of particular interest is a comparison of the apparent linewidths for the $R_1(11)$ transitions from the LIF and photoabsorption spectra. The LIFS linewidths are smaller for two reasons: smaller instrumental bandwidth and smaller Doppler width associated with the lower transition energy. The narrowest $R_1(11)$ line (apparent width 0.15 cm^{-1} FWHM) occurs for the (14,26) LIF spectrum which has the lowest transition energy ($\sim$23 000 cm^{-1}, Doppler width 0.05 cm^{-1} FWHM), followed by the (14,16) LIF spectrum (apparent width 0.18 cm^{-1} FWHM, transition energy $\sim$34 000 cm^{-1}, Doppler width 0.07 cm^{-1} FWHM), and the VUVLS and VUVFTS results for the (14,0) transition (apparent widths 0.21 cm^{-1} and 0.24 cm^{-1} FWHM, respectively, transition energy $\sim$56 000 cm^{-1}, Doppler width 0.12 cm^{-1} FWHM). Nevertheless, when analyzed using the procedures outlined in Sec. III with appropriate instrumental functions, each spectrum implies a consistent Lorentzian F_1 width of $\sim$0.11 cm^{-1} FWHM. Synthetic spectra fitted to each set of measurements, shown in Fig. 1, are seen to accurately reproduce the experimental results. However, we note here that, in order to obtain the fitted VUVFTS cross section in Fig. 1, it was necessary to vary the instrumental resolution from its nominal value. A resolution of 0.19 cm^{-1} FWHM resulted in VUVFTS predissociation linewidths and oscillator strengths in reasonable agreement with the VUVLS values for all three fine-structure components, in agreement with the general discussion in Sec. III C. It may be concluded from this example illustrated in Fig. 1 that, despite the diverse characteristics of the different experimental methods, each technique is capable of producing reliable predissociation linewidths, provided that the instrumental functions are well controlled and monitored. In the case of the VUVFTS measurements, the unexpected and unprecedented degradation of the effective resolution resulted in a lack of monitoring, preventing the independent deduction of a reliable set of linewidths.

The predissociation widths determined for all rotational and fine-structure levels of the B state with $v = 13$ and 14, using the VUVLS and LIFS experimental techniques, are shown in Figs. 2 and 3 and are listed in Tables I and II, respectively. The results are given as a function of the B-state rotational quantum number N, where $N = J - 1$, $N = J$, or $N = J + 1$ for the F_1, F_2, or F_3 fine-structure levels, respectively. Unless indicated otherwise, each tabulated level width represents the average of values determined separately for $P(N+1)$ and $R(N-1)$ transitions terminating on the same B-state level.[44] In a few cases, particularly for lines near the band heads terminating on levels of low rotational quantum number, widths measured for satellite-branch lines have been included in the averages. The listed uncertainties in the level widths include statistical uncertainties reflecting
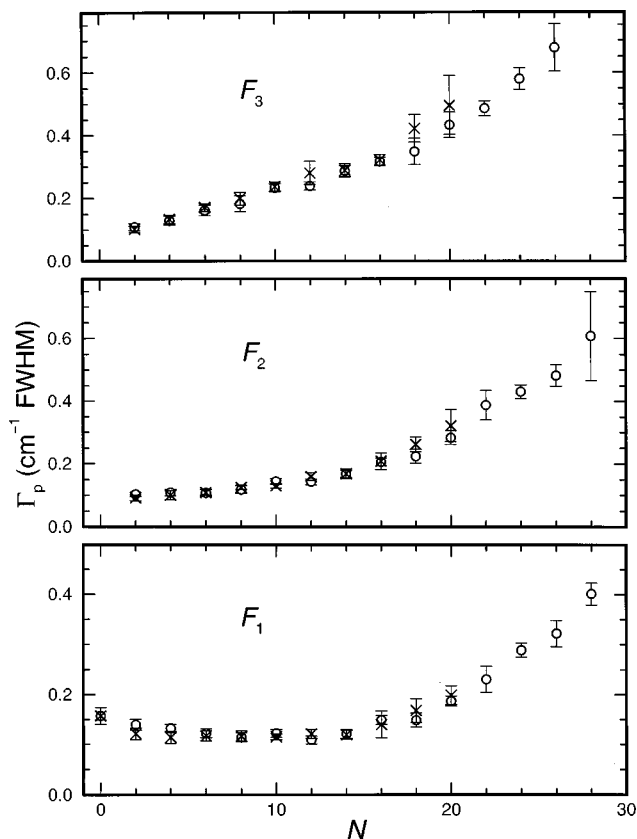

FIG. 2. Measured fine-structure-specific predissociation level widths for $B\,^3\Sigma_u^-(v=13)$ as a function of B-state rotational quantum number N. Each point represents the average obtained from separate P- and R-branch measurements using the VUVLS (circles) and LIFS (crosses) techniques.

the S/N of the measurements and the sensitivity of the least-squares fitting procedure, together with a contribution reflecting incomplete knowledge of the instrumental linewidth. Uncertainty due to the instrumental contribution is smaller in the case of the LIFS results, but this is counterbalanced by an increased uncertainty due to smaller S/N. The VUVLS results cover a greater range of rotation, up to $N = 28$ for $v = 13$ and $N = 30$ for $v = 14$, primarily because of the larger S/N and the fact that measurements have been made using a greater range of O$_2$ pressures. The VUVLS measurements taken at pressures from 10 Torr to 100 Torr, the maximum employed, have been corrected for collisional broadening (0.2 cm^{-1}/atm),[28,29] as indicated in Tables I and II. The LIFS results require no such correction since they were taken at lower pressures.

There is excellent agreement between each set of results: only in the case of the $v = 14$, F_1, $N = 26$ level do the VUVFTS and LIFS linewidths differ by more than the combined experimental uncertainties. This agreement supports the applicability of these experimental techniques to the measurement of narrow linewidths, indicates that the calibrations of the instrumental resolutions have been performed properly, and supports the reliability of the predissociation level widths presented here. The complexity of the rotational and fine-structure dependence of the $B(v = 13$ and 14$)$ level widths is clearly evident from Figs. 2 and 3. The individual level widths vary over an order of magnitude, from

J. Chem. Phys., Vol. 109, No. 10, 8 September 1998
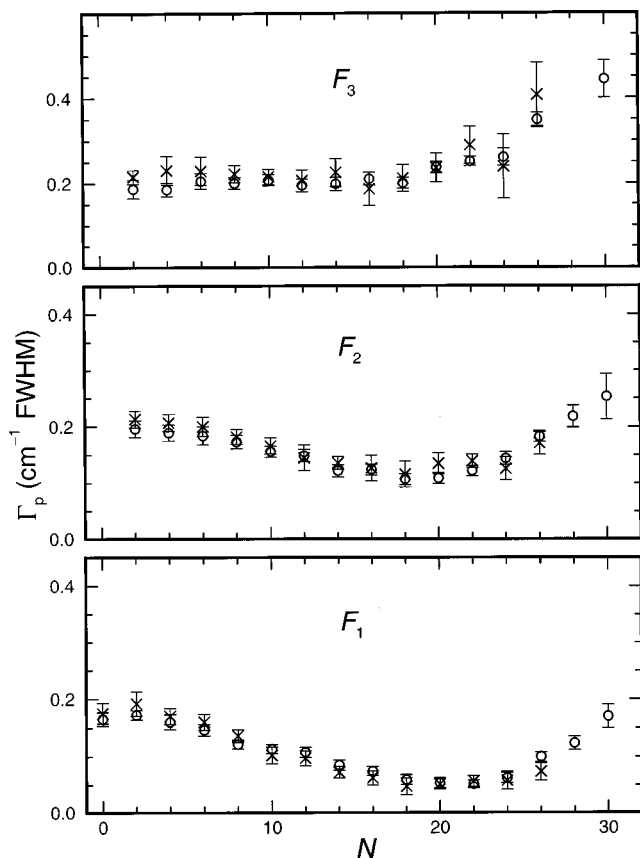
Dooley *et al.* 3865

FIG. 3. Measured fine-structure-specific predissociation level widths for $B\,^3\Sigma_u^-(v=14)$ as a function of B-state rotational quantum number N. Each point represents the average obtained from separate P- and R-branch measurements using the VUVLS (circles) and LIFS (crosses) techniques.

TABLE I. Measured fine-structure-specific predissociation level widths for $B\,^3\Sigma_u^-(v=13, N)$, in cm^{-1} FWHM.

Level	N	VUVLS	LIFS
F_1	0	0.157 ± 0.008	0.157 ± 0.017
	2	0.139 ± 0.011	0.121 ± 0.012
	4	0.132 ± 0.008	0.114 ± 0.012
	6	0.122 ± 0.009	0.117 ± 0.010
	8	0.114 ± 0.009	0.116 ± 0.011
	10	0.122 ± 0.008	0.115 ± 0.006
	12	0.109 ± 0.008	0.121 ± 0.009
	14	0.121 ± 0.009	0.119 ± 0.009
	16	0.149 ± 0.009	0.140 ± 0.027
	18	0.149 ± 0.014[a]	0.168 ± 0.024
	20	0.187 ± 0.010	0.199 ± 0.019
	22	0.231 ± 0.026[b]	
	24	0.289 ± 0.014[c]	
	26	0.322 ± 0.026[c]	
	28	0.401 ± 0.022[c]	
F_2	2	0.103 ± 0.007	0.092 ± 0.009
	4	0.109 ± 0.010	0.100 ± 0.014
	6	0.108 ± 0.011	0.109 ± 0.009
	8	0.118 ± 0.012	0.125 ± 0.007
	10	0.144 ± 0.009	0.130 ± 0.007
	12	0.143 ± 0.009	0.159 ± 0.013
	14	0.168 ± 0.011	0.169 ± 0.015
	16	0.206 ± 0.012	0.209 ± 0.026
	18	0.224 ± 0.022[a]	0.262 ± 0.023
	20	0.284 ± 0.022[a]	0.322 ± 0.052
	22	0.388 ± 0.047[b]	
	24	0.431 ± 0.022[c]	
	26	0.483 ± 0.034[c]	
	28	0.608 ± 0.141[a,c]	
F_3	2	0.110 ± 0.011	0.102 ± 0.010
	4	0.129 ± 0.014	0.134 ± 0.013
	6	0.162 ± 0.017	0.171 ± 0.013
	8	0.183 ± 0.025	0.199 ± 0.020
	10	0.233 ± 0.012	0.237 ± 0.014
	12	0.239 ± 0.013	0.280 ± 0.037
	14	0.286 ± 0.017	0.288 ± 0.021
	16	0.316 ± 0.013	0.321 ± 0.018
	18	0.348 ± 0.042[a]	0.422 ± 0.044
	20	0.433 ± 0.041[a]	0.496 ± 0.094
	22	0.486 ± 0.024[a,c]	
	24	0.580 ± 0.034[c]	
	26	0.678 ± 0.075[c]	

[a]Determined from R-branch line only.
[b]Determined from P-branch line only.
[c]Corrected for collisional broadening.

~ 0.05 cm^{-1} FWHM for $v=14$, F_1, $N\approx20$, to ~ 0.6 cm^{-1} FWHM for $v=13$, F_3, $N=26$. While there is an essentially monotonic increase in level width with rotation for the F_2 and F_3 levels with $v=13$ and the F_3 levels for $v=14$, the remaining fine-structure levels at first decrease in width for increasing rotation, and then increase, passing through the minima near $N=10$ for F_1, $v=13$; $N=20$ for F_2, $v=14$; and $N=22$ for F_1, $v=14$. This general behavior is in good agreement with the predissociation-model predictions of Lewis *et al.*[5] In addition, although, for the reasons discussed in Sec. III C, we are unable to report quantitative VUVFTS linewidths, VUVFTS cross sections analyzed using the nominal instrumental resolution yield widths displaying the same rotational and fine-structure trends as in Figs. 2 and 3.

Prior to this work, there had been very few measurements of fine-structure-specific predissociation level widths for $B(v=13$ and $14)$, none of which was performed at high instrumental resolution. Lewis *et al.*[5] analyzed the photoabsorption cross sections of Yoshino *et al.*,[12] obtaining a few fine-structure-specific widths for $v=13$, $N=18-26$, while Lewis *et al.*[8] reported a few low-resolution fine-structure widths for $v=14$. It is clear from an inspection of Figs. 17 and 18 of Lewis *et al.*[5] that their[5,8] results are insufficient to establish the rotation and fine-structure dependence of the predissociation widths for these narrow vibrational levels. The present study rectifies this deficiency comprehensively,

providing a complete set of fine-structure-specific predissociation level widths for $B(v=13$ and $14)$.

V. CONCLUSIONS

In a comparative study using an array of state-of-the-art high-resolution spectroscopic techniques, the fine-structure and rotation dependencies of the predissociation of the O_2 $B\,^3\Sigma_u^-(v=13$ and $14)$ levels have been characterized completely for the first time. The measurements presented here are the first to have been performed at high resolution for these levels and represent a significant advance on previous knowledge.[5] In combination with similar measurements for other vibrational levels, the present fine-structure-specific results will enable significant refinements in the parameters of

TABLE II. Measured fine-structure-specific predissociation level widths for $B\,^3\Sigma_u^-(v=14,N)$, in cm^{-1} FWHM.

Level	N	VUVLS	LIFS
F_1	0	0.165 ± 0.012[a]	0.175 ± 0.018
	2	0.172 ± 0.008	0.192 ± 0.021
	4	0.160 ± 0.013	0.170 ± 0.014
	6	0.146 ± 0.010	0.160 ± 0.014
	8	0.121 ± 0.008	0.136 ± 0.011
	10	0.113 ± 0.008	0.102 ± 0.015
	12	0.107 ± 0.009	0.097 ± 0.013
	14	0.085 ± 0.009	0.072 ± 0.010
	16	0.074 ± 0.008	0.062 ± 0.013
	18	0.059 ± 0.009	0.047 ± 0.015
	20	0.053 ± 0.009	0.051 ± 0.009
	22	0.051 ± 0.007[b]	0.056 ± 0.010
	24	0.062 ± 0.009[c]	0.057 ± 0.016
	26	0.099 ± 0.008[c]	0.073 ± 0.015
	28	0.123 ± 0.012[c]	
	30	0.170 ± 0.020[b,c]	
F_2	2	0.196 ± 0.015	0.213 ± 0.015
	4	0.189 ± 0.014	0.207 ± 0.015
	6	0.184 ± 0.016	0.200 ± 0.017
	8	0.173 ± 0.012	0.182 ± 0.013
	10	0.156 ± 0.010	0.166 ± 0.014
	12	0.149 ± 0.011	0.145 ± 0.023
	14	0.122 ± 0.011	0.136 ± 0.011
	16	0.124 ± 0.010	0.127 ± 0.023
	18	0.107 ± 0.010	0.116 ± 0.023
	20	0.109 ± 0.010[a]	0.135 ± 0.019
	22	0.122 ± 0.009[b]	0.139 ± 0.012
	24	0.144 ± 0.011[c]	0.126 ± 0.020
	26	0.183 ± 0.010[c]	0.171 ± 0.020
	28	0.218 ± 0.019[b,c]	
	30	0.253 ± 0.040[b,c]	
F_3	2	0.186 ± 0.022	0.215 ± 0.016
	4	0.185 ± 0.016	0.230 ± 0.034
	6	0.205 ± 0.019	0.229 ± 0.033
	8	0.200 ± 0.014	0.222 ± 0.020
	10	0.207 ± 0.013	0.215 ± 0.018
	12	0.195 ± 0.015	0.206 ± 0.026
	14	0.198 ± 0.015	0.225 ± 0.033
	16	0.210 ± 0.015	0.186 ± 0.039
	18	0.200 ± 0.013	0.211 ± 0.032
	20	0.237 ± 0.013	0.236 ± 0.034
	22	0.251 ± 0.011	0.289 ± 0.044
	24	0.261 ± 0.020[c]	0.239 ± 0.076
	26	0.349 ± 0.016[c]	0.406 ± 0.076
	30	0.443 ± 0.044[b,c]	

[a]Determined from *P*-branch line only.
[b]Determined from *R*-branch line only.
[c]Corrected for collisional broadening.

the standard model[1,2,5] for predissociation of the *B* state, resulting in greatly improved predictive capabilities and more reliable photochemical models of the terrestrial atmosphere. Although it was not possible to determine quantitative linewidths using the VUVFTS technique, the degree of agreement between the linewidths measured using the VUVLS and LIFS techniques is satisfying and gives confidence in the applicability of the experimental methods and the reliability of the results. However, the high-resolution performance provided by each technique was achieved at the cost of considerable experimental complexity and difficult adjustments and calibrations. In particular, each experimental technique

suffers, to a greater or lesser extent, from ill definition of the instrumental resolution which must be carefully controlled and monitored. Further research into the detailed instrumental line shapes is warranted.

[1] P. S. Julienne and M. Krauss, J. Mol. Spectrosc. **56**, 270 (1975).
[2] P. S. Julienne, J. Mol. Spectrosc. **63**, 60 (1976).
[3] M. Nicolet and P. Mange, J. Geophys. Res. **59**, 15 (1954).
[4] K. Minschwaner, G. P. Anderson, L. A. Hall, and K. Yoshino, J. Geophys. Res. **97**, 10103 (1992).
[5] B. R. Lewis, S. T. Gibson, and P. M. Dooley, J. Chem. Phys. **100**, 7012 (1994).
[6] B. R. Lewis, L. Berzins, and J. H. Carver, J. Quant. Spectrosc. Radiat. Transfer **36**, 209 (1986).
[7] K. Yoshino, D. E. Freeman, J. R. Esmond, and W. H. Parkinson, Planet. Space Sci. **31**, 339 (1983).
[8] B. R. Lewis, L. Berzins, J. H. Carver, and S. T. Gibson, J. Quant. Spectrosc. Radiat. Transfer **36**, 187 (1986).
[9] A. S.-C. Cheung, K. Yoshino, J. R. Esmond, S. S.-L. Chiu, D. E. Freeman, and W. H. Parkinson, J. Chem. Phys. **92**, 842 (1990).
[10] K. Yoshino, D. E. Freeman, J. R. Esmond, and W. H. Parkinson, Planet. Space Sci. **35**, 1067 (1987).
[11] A. S.-C. Cheung, K. Yoshino, W. H. Parkinson, and D. E. Freeman, Can. J. Phys. **62**, 1752 (1984).
[12] K. Yoshino, J. R. Esmond, A. S.-C. Cheung, D. E. Freeman, and W. H. Parkinson, Planet. Space Sci. **40**, 185 (1992).
[13] P. C. Cosby, H. Park, R. A. Copeland, and T. G. Slanger, J. Chem. Phys. **98**, 5117 (1993).
[14] R. A. Copeland, P. C. Cosby, D. R. Crosley, J. B. Jeffries, and T. G. Slanger, J. Chem. Phys. **86**, 2500 (1987).
[15] A. M. Wodtke, H. Hüwel, H. Schlüter, H. Voges, G. Meijer, and P. Andresen, J. Chem. Phys. **89**, 1929 (1988).
[16] X. Yang, A. M. Wodtke, and L. Hüwel, J. Chem. Phys. **94**, 2469 (1991).
[17] B. R. Lewis, S. T. Gibson, K. G. H. Baldwin, and J. H. Carver, J. Opt. Soc. Am. B **6**, 1200 (1989).
[18] P. M. Dooley, B. R. Lewis, S. T. Gibson, and K. G. H. Baldwin, J. Electron Spectrosc. Relat. Phenom. **80**, 29 (1996).
[19] B. R. Lewis, P. M. Dooley, J. P. England, K. Waring, S. T. Gibson, K. G. H. Baldwin, and H. Partridge, Phys. Rev. A **54**, 3923 (1996).
[20] R. Hilbig and R. Wallenstein, IEEE J. Quantum Electron. **QE19**, 194 (1983).
[21] K. Yamanouchi and S. Tsuchiya, J. Phys. B **28**, 133 (1995).
[22] B. R. Lewis, J. P. England, R. J. Winkel, Jr., S. S. Banerjee, P. M. Dooley, S. T. Gibson, and K. G. H. Baldwin, Phys. Rev. A **52**, 2717 (1995).
[23] K. Yoshino, D. E. Freeman, and W. H. Parkinson, J. Phys. Chem. Ref. Data **13**, 207 (1984).

[24] S. Gangopadhyay, N. Melikechi, and E. E. Eyler, J. Opt. Soc. Am. B **11**, 231 (1994).

[25] M. S. Fee, K. Danzmann, and S. Chu, Phys. Rev. A **45**, 4911 (1992).

[26] J. W. Hepburn, *Vacuum Ultraviolet Photoionization and Photodissociation of Molecules and Clusters*, edited by C. Y. Ng (World Scientific, Singapore, 1991), p. 446.

[27] R. M. Goody, *Atmospheric Radiation. I. A Theoretical Basis* (Clarendon, Oxford, 1964), pp. 125–138.

[28] B. R. Lewis, L. Berzins, C. J. Dedman, T. T. Scholz, and J. H. Carver, J. Quant. Spectrosc. Radiat. Transfer **39**, 271 (1987).

[29] P. M. Dooley, B. R. Lewis, K. Waring, S. T. Gibson, and K. G. H. Baldwin, J. Quant. Spectrosc. Radiat. Transfer **58**, 93 (1997).

[30] H. Park and T. G. Slanger, J. Chem. Phys. **100**, 287 (1994).

[31] S. Gerstenkorn and P. Luc, *Atlas du Spectre d'Absorption de la Molécule de l'Iode Entre 14800–20000 cm^{-1}* (Editions du C.N.R.S., Paris, 1978); *Atlas du Spectre d'Absorption de la Molécule de l'Iode Entre 14800–20000 cm^{-1}, Complément: Identification des Transitions du Système (B-X)* (Editions du C.N.R.S., Paris, 1980). A multiplicative correction factor of 0.999 999 62 was applied to the reported line positions as recommended by these authors.

[32] J. Cariou and P. Luc, *Atlas du Spectre d'Absorption de la Molécule de Tellure Partie 2: 18500–21200 cm^{-1} and Partie 5: 21100–23800 cm^{-1}* (Laboratoire Aime-Cotton, CNRS II, Orsay, 1980).

[33] A. P. Thorne, C. J. Harris, I. Wynne-Jones, R. C. M. Learner, and G. Cox, J. Phys. E **20**, 54 (1987).

[34] A. P. Thorne, Phys. Scr. **T65**, 31 (1996).

[35] J. E. Murray, K. Yoshino, J. R. Esmond, W. H. Parkinson, Y. Sun, A. Dalgarno, A. P. Thorne, and G. Cox, J. Chem. Phys. **101**, 62 (1994).

[36] K. Ito, T. Namioka, Y. Morioka, T. Sasaki, H. Noda, K. Goto, T. Katayama, and M. Koike, Appl. Opt. **25**, 837 (1986).

[37] While the effects of spontaneous radiative emission provide a negligible lifetime-broadening contribution to the Lorentzian linewidth, of course the LIFS experiment would not be possible without this process.

[38] It is assumed that there are no correlations between the individual broadening processes.

[39] Since the effective vibrational oscillator strength varies insignificantly with the fine-structure component for lines with a given N', the relative fine-structure photoabsorption line strengths are determined completely by the respective Boltzmann and Hönl-London factors. Both of these factors may be calculated to a high degree of accuracy: the Boltzmann factors may be derived from the well known ground-state term values for O_2 [L. Veseth and A. Lofthus, Mol. Phys. **27**, 511 (1974)], while expressions for the appropriate intermediate-coupling case [J. B. Tatum and J. K. G. Watson, Can. J. Phys. **49**, 2693 (1971)] may be used with the ground- and upper-state term values (Ref. 23) to calculate the Hönl-London factors.

[40] The attribution in Ref. 13 of unexpectedly large Gaussian linewidths to a relatively high translational temperature of the absorbing O_2 is incorrect. Subsequent studies of the LIFS line shapes as a function of pressure and of time delay between the pump and probe laser beams found that the O_2 was in thermal equilibrium with the buffer gas (300 K). A more likely explanation for these earlier results is an unexpectedly large probe-laser bandwidth.

[41] As described in Ref. 13, the relative absorption line strengths were calculated from the eigenvectors obtained in a diagonalization of the effective Hamiltonians for the B- and X-state levels, assuming a 300 K thermal population distribution in the X-state rotational levels. This procedure is equivalent to that described in Ref. 39.

[42] J. W. Brault (private communication).

[43] R. C. M. Learner and A. P. Thorne, J. Opt. Soc. Am. B **5**, 2045 (1988).

[44] Since LIFS measurements were made on several bands with various v'', the corresponding linewidth averages include multiple transitions accessing each upper-state level.